Preprint Title	Functionalization of nZVI nanoparticles with dipicolinic acid by one-pot synthesis -and testing of PDCA-nZVI material properties in cadmium removal from water
Authors	Sanda Roncevic, Ivan Nemet, Viktor Zagorec and Atiđa Selmani
Publication Date	10 Jan 2020
Article Type	Full Research Paper
ORCID® iDs	Sanda Roncevic - https://orcid.org/0000-0002-1899-6382; Atiđa Selmani - https://orcid.org/0000-0002-5830-2138

Functionalization of nZVI nanoparticles with dipicolinic acid by one-pot synthesis and testing of PDCA-nZVI material properties in cadmium removal from water

Sanda Rončević [1)*], Ivan Nemet [1)], Viktor Zagorec [1)], Atiđa Selmani [2)]

1) Department of Chemistry, Faculty of Science, University of Zagreb, Horvatovac 102a, 10000 Zagreb, Croatia
2) Institute Ruđer Bošković, Bijenička cesta 54, 10000 Zagreb, Croatia

* Corresponding author

Email: Sanda Rončević - roncevic@chem.pmf.hr

Abstract

The low-cost method of functionalization of zero-valent iron nanoparticles (nZVI) by dipicolinic acid (PDCA) by one-pot synthesis was studied in this work. The chemical reduction of iron salt with concurrent addition of ligand was performed using different molar ratio of starting reagents. Functionalization of nZVI was confirmed by FT-IR spectroscopy. The formation of oxide layers on the core of iron particles that consists of magnetite and feroxyhyte was confirmed by the XRD method. Morphology of obtained material was examined by SEM study and it revealed the formation of short-chains of spherical particles by use of equimolar ratio of reactants. The appearance of ellipsoidal aggregates was observed by use of reagents molar ratio of 1/2. The performance characteristics of obtained materials were tested in cadmium removal from water solutions. Concentrations of cadmium in solutions were determined by ICP-OES measurements. The efficiency of removal of cadmium was tested on bare nZVI particles, one-pot synthetized PDCA-nZVI particles, and particles obtained by subsequent incubation of PDCA onto nZVI. The results of the measured hydrodynamic diameter and zeta-potential in solutions were correlated with adsorption characteristics of prepared functionalized materials. The most efficient adsorption of cadmium was observed by exploiting PDCA-nZVI nanomaterial that was obtained from one-pot synthesis.

Keywords

nZVI; dipicolinic acid; functionalization; one-pot synthesis; Cd^{2+} removal

Introduction

Among the many types of engineered nanomaterials zero-valent iron nanoparticles (nZVI) demonstrated a great potential in different fields of application. High reactivity and large surface area of environment-friendly and cost-effective nZVI particles are mostly exploited in removal of heavy metals and organic pollutants from water and soil systems [1-3]. Due to core-shell structure of nZVI particles, the removal of pollutants occurs through mechanisms of adsorption, reduction and complexation [4-6]. However, the strong agglomeration potential and rapid sedimentation complicate handling and applicability of nZVI particles in remediation purposes [7, 8]. For this reason, a various methods of surface modification of nZVI have been studied. By chemical functionalization of surface, the enhancements of colloidal stability and better control of their reactivity are often achieved [9-11]. The strategies of nZVI surface alteration are generally focused on selection of suitable carriers such as surfactants, polymers or inorganic materials; and/or to the selection of suitable capping agents for coating of the particle surface [12].

Metal-binding organic ligands such as 2,6-pyridinedicarboxylic acid or dipicolinic acid (PDCA) are widely used as capping or extractive reagents for transition and rare earth metals. Dipicolinic acid and its derivatives are often used as on-line complexing reagents in ion chromatography for transition metals speciation [13-16]. Furthermore, dipicolinic acid and its derivatives are being featured as ligands in coordination complexes for pharmaceutical use [17] and bioimaging applications. The most recent approaches utilize the novel hybrid materials supported with PDCA in separation of elements of lanthanides and actinides series [19-21]. Mahmoud and coauthors reported the excellent efficiency of novel nanocomposite material, which combines the

magnetic characters of nZVI and selectivity of incorporated organic ligand in removal of bivalent transition metals and selected radionuclides from water [20]. The functionalization of nZVI surface with PDCA was the object of our previous study where we observed the changes of nZVI particle shape [22]. The elongation of particles in ellipsoidal forms of reduced size occurred by variation of molar ratio of iron and PDCA during the synthesis. It was also demonstrated that changes of particle size and shape affect the metal ions removal from water solutions.

In the present work, the focus of our investigation is comparison of nZVI and functionalized PDCA-nZVI material characteristics. The functionalized materials were prepared through one-pot synthesis procedure. Molar ratio of iron and PDCA reagents was adjusted to 1:1 and 2:1. The main goal of described experiments is to set up the efficient and low-cost method for functionalization of nZVI particles with dipicolinic acid. The characterization of obtained materials was performed by dynamic light scattering (DLS), infrared spectroscopy (FT-IR), X-ray diffraction (XRD) and scanning electron microscopy (SEM). Another objective of this work is to test a practical applicability of synthesized nanomaterials. For this reason, the efficiency of metal ion removal from water solutions was tested on cadmium ions by using inductively coupled plasma optical emission spectrometry (ICP-OES). In order to estimate the removal efficiency of material obtained through one-pot synthesis, the comparison was performed by use of PDCA-nZVI material obtained by incubation. The same molar ratio of reagent was used in separate experiments of incubation of ligand onto nZVI surface. The cadmium removal efficiency of the synthetized types of PDCA-nZVI nanomaterial was compared to cadmium removal of bare nZVI particles and the observed effects are discussed in this work.

Materials and Methods

Synthesis of nZVI particles

Synthesis of bare nZVI particles was performed by sodium borohydride ($NaBH_4$) reduction using a low-cost methodology. The preparation was performed in an open vessel at regular atmospheric conditions, as was reported earlier [22]. The starting solution was prepared by dissolution of 1 g of $FeCl_3 \times 6H_2O$ in 100 mL of deionized distilled water in a 400 mL beaker. An amount of 0.70 g of $NaBH_4$ was dissolved in 100 mL of water. The pH of reaction solution was adjusted to neutral. Freshly prepared solution of $NaBH_4$ was added in droplets into the iron chloride solution under vigorous stirring. The black precipitate appeared immediately after the first addition of $NaBH_4$. After 20 min of stirring, the magnetic precipitate was separated using an external magnet and washed with deionized distilled water. Prepared bare nZVI particles were stored in containers under ethanol to prevent further oxidation.

One-pot synthesis of PDCA-nZVI particles

Solution of dipicolinic acid (2,6-pyridinedicarboxylic acid; PDCA) was prepared by dissolution of 0.7112 g of pure compound in 150 mL of deionized distilled water. Due to the poor solubility of PDCA, the solution was prepared by use of ultrasonic bath. Solution was placed into beaker containing dissolved iron chloride and the pH of solution was adjusted to neutral by addition of several drops of sodium hydroxide solution. The reduction process was performed by addition of $NaBH_4$ solution during stirring. The black precipitate of magnetic nanoparticles formed instantaneously after addition of the reducing reagent. The PDCA-nZVI particles were filtered, re-flushed with water and stored under ethanol. The experiment was performed using the molar ratio PDCA/Fe = 1/1 and the ratio PDCA/Fe = 1/2. The last one was prepared by use

of 0.3556 g PDCA dissolved in 150 mL of water. Black coloured magnetic particles were formed with both of applied concentrations.

Characterization of synthetized nanoparticles

Particle morphology was observed by scanning electron microscopy (SEM) on a Thermo Fisher Scientific FEI Quanta 250 FEG. The images were obtained operating in high vacuum mode (10^{-4} Pa - 30^{-3} Pa) on Au-Pt coated samples using secondary electrons detector (Everhart Thornley Detector, ETD) and acceleration voltage of 7 to 10 kV. Infrared spectra were obtained from KBr pellets using FTIR Bruker Vector 22 in the wave range of 4000-450 cm^{-1} (50 scans acquisition, resolution 4 cm^{-1}). Crystalline phases were determined by powder X-ray diffraction on a Philips X'Pert diffractometer (2θ range 15° - 100°) in the Bragg–Brentano geometry using Cu Kα radiation. The samples were placed on Si sample holders. Patterns were visualized using the X'Pert program HighScore. The size distribution of particles was determined by means of dynamic light scattering (DLS) an electrophoretic light scattering (ELS) using a photon correlation spectrometer equipped with a 532 nm "green" laser (Zetasizer Nano ZS, Malvern Instruments, Worcestershire, UK). The intensity of scattered light was detected at the angle of 173°. The hydrodynamic diameter (d_H) was obtained as a value at the peak maximum of the particle-size volume-distribution function. Each sample was measured six times, and representative data are shown. Characteristic ζ-potential values were calculated from the measured electrophoretic mobility. Results are expressed as an average value of three measurements. All measurements were conducted at (25.0 ± 0.1) °C. The data were processed by the Zetasizer software 6.32 (Malvern Instrument Worcestershire, UK).

The ICP-OES analyses of solutions from adsorption experiments were performed with a Teledyne Leeman Labs. Prodigy High Dispersion ICP. The instrument is equipped

with 40 MHZ “free-running” radiofrequency generator and echelle grating spectrometer with a large-format programmable array detector (L-PAD). Sample introduction system consists of a peristaltic pump, glass cyclonic spray chamber, glass concentric nebulizer and a dual-view torch. The solution uptake rate was adjusted on 1 mL min^{-1}. The radiofrequency power of 1.2 kW, and flow rates of argon (coolant 18 L min^{-1}, auxiliary 0.9 L min^{-1}) were held constant during measurements. Ionic and atomic emission lines of cadmium at 214,441 and 228,802 nm were selected from image on L-PAD detector as the best ones i.e. lines without spectral and background interferences. Measured detection limits comprised the values of 0.2 µg L^{-1} and 0.3 µg L^{-1}. All calibration standards were prepared by appropriate dilution of cadmium standard stock solution in the concentration range from 0.1 to 100 mg L^{-1}. Nitric acid was added in each calibration solution up to the final concentration of 2 % *v*/*v*.

Adsorption experiments

Cadmium solutions in the concentration range of 0.1 – 50 mg L^{-1} were prepared from the standard stock solution of spectral purity (Plasma Pure, Leeman Labs, Hudson, NH, USA). An amount of 10 mg of synthetized nanoparticles was placed into glass vials where the volume of 10 mL of cadmium solutions was added. Glass vials were covered with a glass lid and were sonicated for 30 min in an ultrasonic bath. Removal of supernatant was performed after centrifugation and by use of external magnet. Metal concentrations were measured directly from filtered solutions by the ICP-OES method. Nanoparticles that remained in vials were dissolved by addition of 1 mL of concentrated nitric acid and 0.1 mL of concentrated hydrochloric acid. The obtained solutions were diluted to 25 mL with distilled deionized water. Concentration of cadmium in these solutions denotes adsorption on nZVI particles and it was determined by the ICP-OES method.

In order to compare the removal efficiency of one-pot synthetized PDCA-nZVI material, another set of particles was prepared by incubation of PDCA in suspension of nZVI. For this purpose, bare nZVI particles were synthesized according to the procedure described above. The flushed magnetic precipitate is replaced into 300 mL conical flask with ground glass stopper. The prepared solution of 0.7112 g of PDCA in 150 mL of deionized distilled water was added into flask. The flask was inserted in ultrasonic bath and sonication was performed during 30 minutes. The precipitate that contained particles of molar ratio PDCA/Fe = 1/1 was removed from the solution by magnetic separation and stored in ethanolic solution. The same procedure was repeated by use of 0.3556 g PDCA in 150 mL of water to form particles of molar ratio PDCA/Fe = 1/2. The obtained bare nZVI particles and PDCA functionalized nZVI nanoparticles are showed in Figure 1. The adsorption test was repeated separately for each type of synthetized nanoparticles, i.e. bare nZVI and functionalized PDCA-nZVI particles obtained from one-pot synthesis and incubation in solutions.

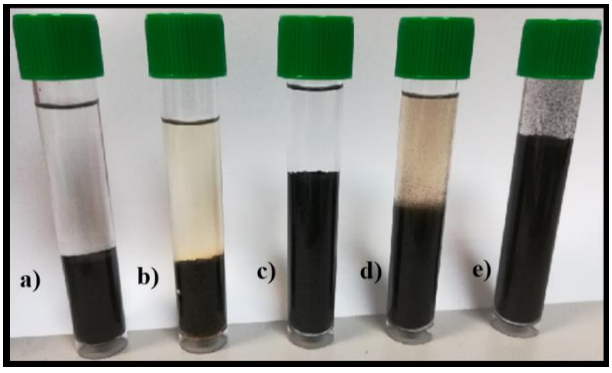

Figure 1. Synthetized nanomaterials: a) non-functionalized zero-valent iron nanoparticles (nZVI); b) PDCA-nZVI 1/1 from one-pot synthesis; c) PDCA-nZVI 1/1 obtained by incubation; d) PDCA-nZVI 1/2 from one-pot synthesis; e) PDCA-nZVI 1/2 obtained by incubation

Results and Discussion

Characterization of PDCA-nZVI particles from one-pot synthesis

Functionalized PDCA-nZVI materials, which were prepared by one-pot synthesis in molar ratio 1:1 and 1:2 were examined by FTIR spectroscopy. The resulting spectra are showed in Figure 2. The spectrum of PDCA-nZVI 1/1 particles shows the appearance of aromatic C-C fundamental vibration at 1058 cm^{-1} and overtone vibration near 2061 cm^{-1}. Absorption band of O-H vibration is visible at 3444 cm^{-1}. There are also present asymmetric and symmetric stretching of COO^- at 1636 and 1391 cm^{-1}, respectively. Stretching vibration of Fe-O appears at 674 cm^{-1}. The product PDCA-nZVI of molar ratio 1/2 shows similar absorption bands in FTIR spectrum. Additional Fe-O vibration at 457 cm^{-1} becomes visible in this material, while in the product of molar ratio 1/1 is missing. The appearance of two bands that are attributed to Fe-O vibrations is described earlier in several studies of removal of organic dyes [23, 24]. Its appearance was explained through the formation of iron oxides on the surface of particles such as magnetite and maghemite. Besides the oxide formation, the appearance of prominent vibrational bands of PDCA, which we observed in FTIR spectra of PDCA-NZVI 1/1 and 1/2 confirmed the capping of ligand on iron particles surface.

a) b)

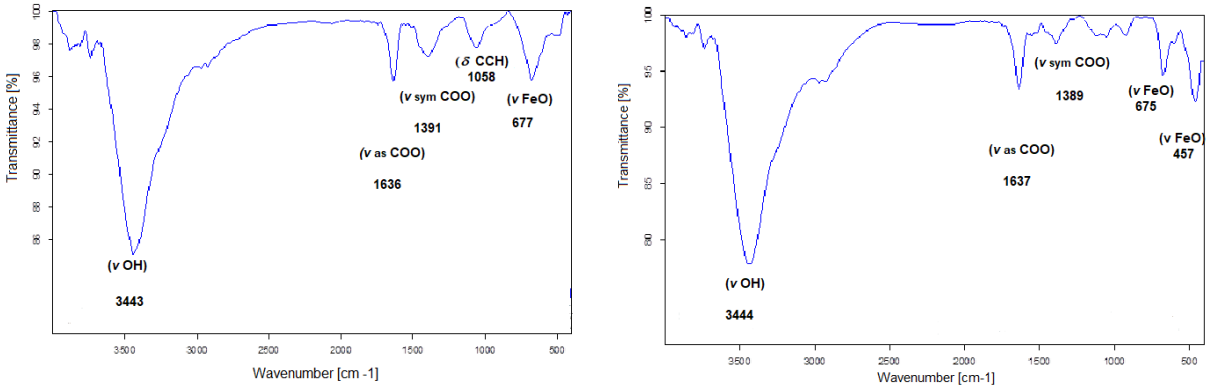

Figure 2. FTIR spectra of nZVI particles after functionalization by dipicolinic acid: a) PDCA-nZVI 1/1; b) PDCA-nZVI 1/2

Diffraction patterns of bare and functionalized particles obtained by XRD are showed in Figure 3. Characteristic maximum at $2\theta = 45°$ in the pattern of freshly-prepared and dried nZVI particles represents the zero-valent iron (α-Fe). Ethanolic suspension of iron particles showed the same diffraction pattern. There are no additional maxima which could imply oxidation process on the particle surface. The corrosion of particles in ethanolic solution is significantly reduced comparing to air-dried particles. Beside the use of ethanol, iso-propanol is also described as a protective layer for nZVI particles [25]. The stability of stored particles is recently studied by Ahmed and authors who showed that extended storage with no corrosion on nZVI particles was achieved using polyvinyl pyrrolidone [4]. We observed the same and unchanged XRD pattern of ethanolic suspension after one month from preparation.

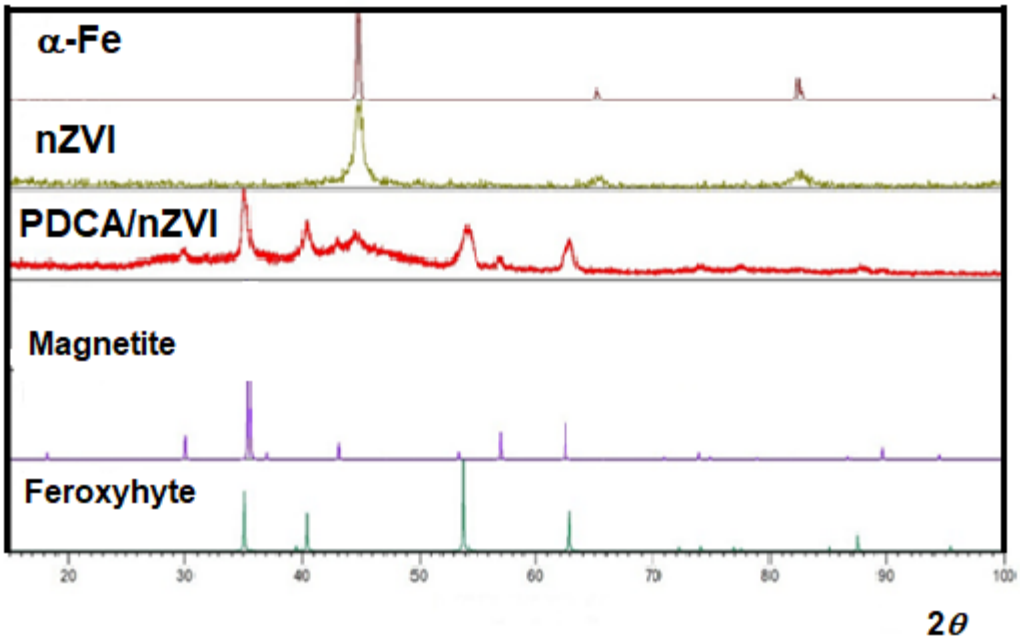

Figure 3. XRD diffraction pattern of: dry nZVI particles; nZVI particles in ethanolic solution; functionalized PDCA-nZVI particles; magnetite (26410-ICSD) and feroxyhyte (38299-ICSD)

In the diffraction pattern of PDCA functionalized particles we observed the remaining peak of α-Fe. By changing of molar ratio of PDCA and iron, there were no visible differences in XRD spectra of obtained materials. The appearance of magnetite (Fe_3O_4) and feroxyhyte (δ-FeOOH) was confirmed from the obtained patterns [22]. Several studies were focused on condensing of iron oxides at different experimental conditions. They showed the great diversity of physicochemical conditions on growth of iron oxide phases [26, 27]. For example, Jolivet et al. concluded that despite of careful control of the size and dispersion of the particles, iron based materials might reveal some unexpected phenomena [26]. The formation of feroxyhyte, such as was found in our work, was explained through conversion of atomic layers of magnetite into maghemite [28]. The authors stated that conversion of magnetite into feroxyhyte is

thermodynamically feasible at nanoscale regarding its similar Gibbs free energy and enthalpy with maghemite (γ-Fe_2O_3). They also found that the formation of feroxyhyte is prevailing in epitaxial layer of nanoparticles. Here we can observe that functionalization of nZVI particles with PDCA at regular atmospheric conditions and using one-pot synthesis procedure leads to formation of zero-valent iron core and oxidized shell of particles, which consists of magnetite and feroxyhyte.

Morphology of obtained particles was observed using SEM method and it is presented in Figure 4. Bare nZVI particles appears as nanospheres with the average diameter of 115 nm. Magnetic dipole-dipole interactions lead to adherence of spheres and they formed chain-like structures.

a)

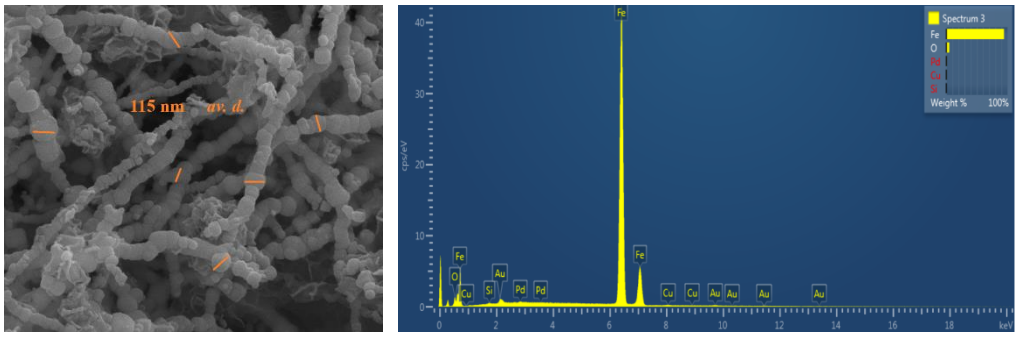

b)

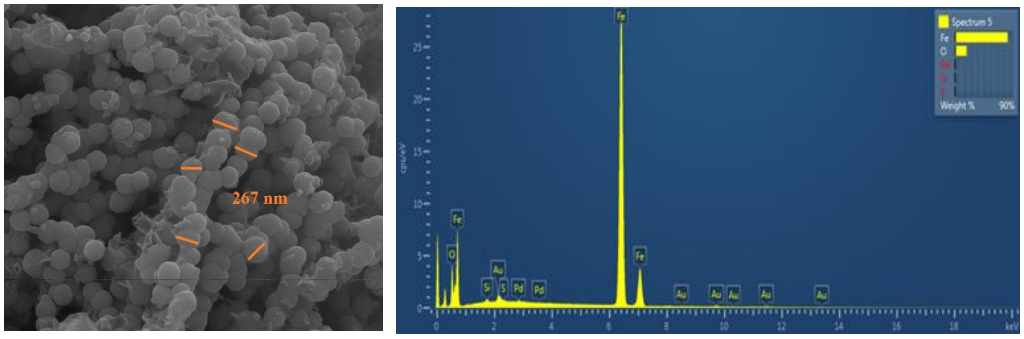

c)

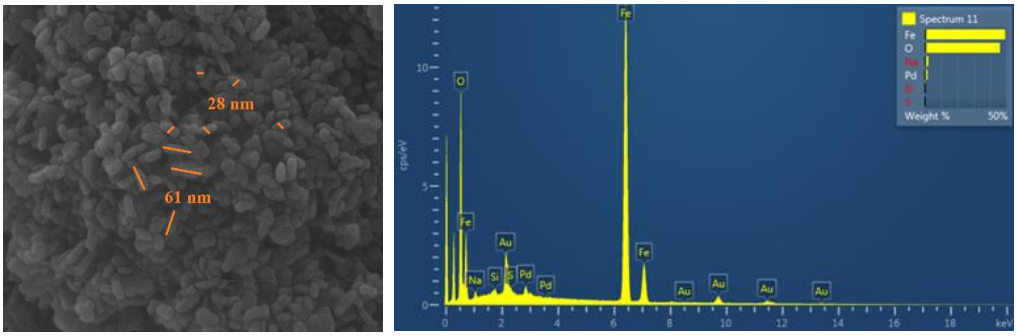

Figure 4. SEM images of synthetized nanoparticles and SEM-EDS mapping of elements content in synthetized nanoparticles: a) non-functionalized zero-valent iron nanoparticles (nZVI); b) PDCA-nZVI 1/1 from one-pot synthesis; c) PDCA-nZVI 1/2 from one-pot synthesis

(The image 4a) (left part), 4b) (both), 4c) (left part) were taken in an adapted way from "Characterization of nZVI nanoparticles functionalized by EDTA and dipicolinic acid: a comparative study of metal ion removal from aqueous solutions" ([Ref. 22]; https://doi.org/10.1039/C9RA04831F), published by The Royal Society of Chemistry under the CC-BY 3.0 unported license, https://creativecommons.org/licenses/by/3.0/; authors: Sanda Rončević, Ivan Nemet, Tea Zubin Ferri, and Dubravka Matković-Čalogović.)

Addition of PDCA during the reduction of iron salts in molar ratio 1/1 caused the formation of nanospheres with average diameter of 267 nm. The long chain-like structure as was observed in bare nZVI material is changed into shorter chains of functionalized particles. The functionalization with PDCA using molar ratio 1/2 caused formation of ellipsoids with average length of 61 nm and average width of 28 nm. The chain-like structure was converted completely into piles and clusters of smaller particles.

The SEM-EDS analysis of particles reveals its oxygen content. From the obtained elemental pattern (Fig. 4.) it could be observed that the mass fraction of oxygen in bare nZVI is almost negligible, while it rises in functionalized particles. Functionalized PDCA-nZVI material of molar ratio 1/1 shows oxygen mass fraction of 21 %. PDCA-nZVI material obtained in ratio 1/2 shows much greater contribution of oxygen (w = 50 %). The complexity of formation of iron oxide films obtained by chemical reduction or spray deposition techniques was examined in several studies [29, 30]. The authors explained that formation of magnetite, maghemite and feroxyhyte depends on thickness of layers and on reaction parameters. By knowing the complex variability of iron oxides appearance at nanoscale, the difference in oxygen content that we observed by functionalization of iron particles with PDCA becomes more understandable. The particle structure on nanoscale is related to different physicochemical conditions. Thus, Nishida et al. demonstrate the formation of spherical feroxyhyte particles into gelatine under inert conditions [30]. Aging of iron-oxide at ambient-air conditions led to formation of needle-like particles, which they explained by rapid oxidation of magnetite into feroxyhyte. The similar properties we observed in functionalized PDCA-nZVI materials. The use of ligand in lower molar ratio caused the appearance of elongated structures.

Adsorption of Cd on PDCA-nZVI nanoparticles

Prepared PDCA-nZVI particles were used as a sorbent material in cadmium removal experiments. In order to compare the removal efficiency of nanomaterial obtained by one-pot synthesis, the additional set of incubated PDCA onto nZVI particles were used in adsorption experiments. The concentration of cadmium in water solution and in solution of dissolved particles was measured by ICP-OES method. The percentage of

adsorbed cadmium at fixed mass of applied particles (0.01 g) and at different cadmium concentration is presented in Figure 5.

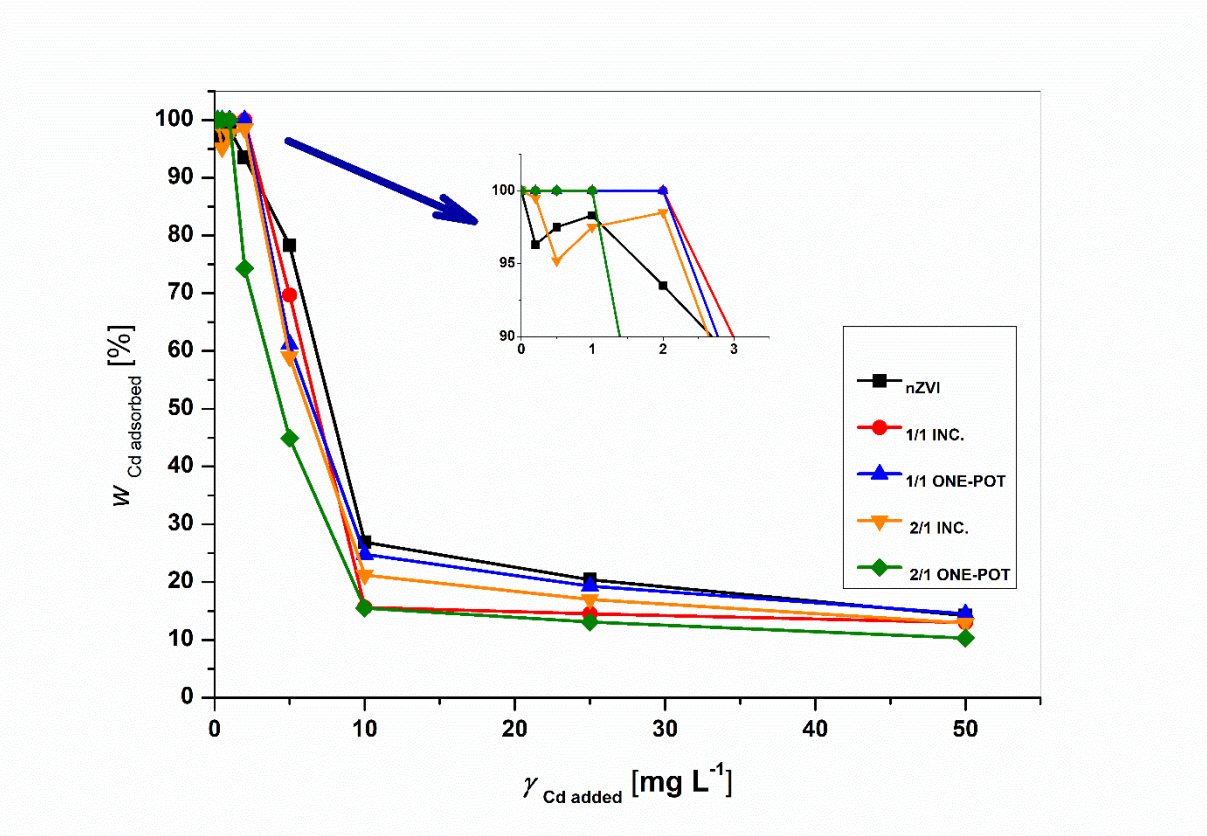

Figure 5. Cadmium ions removal from water solution measured by ICP-OES after adsorption on bare and functionalized nZVI particles

It is obvious that sorption of cadmium on 10 mg of nanoparticles rapidly decreased by rising of cadmium content in solution. Complete removal was achieved in cadmium concentration range of 0.1 – 3 mg L^{-1}. Obtained curves show slightly different slopes depending on type of applied sorbents. The best example of distinction between efficiency of prepared nanomaterials is visible at concentration of 5 mg L^{-1} of cadmium added. At this point, the adsorption is the most efficient on bare nZVI particles (79 %), while it lowered on PDCA-nZVI material. The incubated PDCA-NZVI particles of 1/1 and 1/2 molar ratio showed cadmium removal of 70 % and 60 %, respectively. One-

pot synthetized PDCA-nZVI materials showed that 60 % of cadmium was adsorbed by exploiting spherical PDCA-nZVI 1/1 particles. The ellipsoidal shaped PDCA-nZVI 1/2 showed that 45 % of cadmium was adsorbed from water solution. By rising of concentration of added cadmium (10 - 50 mg L^{-1}), the distinction between sorption of applied different PDCA-nZVI materials becomes almost negligible. For comparison, some recent studies on use of functionalized nZVI or iron oxides as a sorbent for cadmium removal are focused on their maximum efficiency [7, 10, 11, 31]. However, the different loads of nanoparticle material were used in their experimental setup. The range of applied nanomaterial mass usually comprise the values between 100 – 1000 mg, and the studies are mainly directed to examine the cadmium adsorption in the range of 10 – 450 mg L^{-1} [25, 32]. Boparai et al. used thermodynamic parameters to count the maximum adsorption capacity of bare nZVI for cadmium, which takes 769.2 mg g^{-1} [25]. They used material that was synthetized under controlled and inert conditions and it contains particles of 20-200 nm in size. From this study, they conclude that prevailing mechanism of adsorption process of cadmium is chemisorption.

In our work, the sensitive detection of ICP-OES instrument allows the insight in the sorption of low concentration levels of cadmium. The adsorption of cadmium in concentration range bellow 3 mg L^{-1} is showed as magnified graph on Figure 5. The measurements confirmed that the most efficient adsorption occurred by use of one-pot synthetized PDCA-nZVI materials. The saturation effect becomes visible at 1 mg L^{-1} in the case of one-pot PDCA-nZVI 1/2 usage and at 2 mg L^{-1} with PDCA-nZVI 1/1. The bare nZVI and incubated PDCA-nZVI particles showed deviations in cadmium sorption at low concentration range. In order to explain the observed differences, the dynamic light scattering (DLS) method was applied on solutions containing 0.5 and 5 mg L^{-1} of cadmium and 10 mg of prepared nanomaterial. The measured results are presented in Table 1.

Table 1. Hydrodynamic diameter (d_H) of nanoparticles in water solutions containing cadmium ions; γ (Cd) = 0.5 mg L^{-1} and γ (Cd) = 5 mg L^{-1}

Particles	**Bare nZVI** d_H (nm) (%mean volume)	**One-pot PDCA-nZVI 1/1** d_H (nm) (%mean volume)	**One-pot PDCA-nZVI 1/2** d_H (nm) (% mean volume)	**Incubated PDCA-nZVI 1/1** d_H (nm) (% mean volum**e)**	**Incubated PDCA-nZVI 1/2** d_H (nm) (% mean volume)
γ (Cd) 0.5 mg L^{-1}	719.7±214.2 **(100.0)**	315.3±62.8 **(3.0)** 1042.1±110.0 **(80.3)** 5105.5±304.9 **(16.2)**	577.0±51.2 **(93.0)** 5190.2±104.1 **(7.0)**	1053.4±185.5 **(100.0)**	184.3±23.3 **(3.1)** 667.4±206.8 **(95.4)** 5476.5±19.1 **(1.53)**
γ (Cd) 5 mg L^{-1}	169.9±64.2 **(10.7)** 947.6±150.5 **(71.8)** 4439.8±289.5 **(14.9)**	197.2 ±18.7 **(5.8)** 921.4±86.0 **(83.8)** 4545.0±550.8 **(10.4)**	114.1±47.8 **(12.7)** 582.4±200.9 **(70.4)** 4965.4±201.5 **(11.3)**	1766.3±210.9 **(100.0)**	188.0±8.2 **(10.1)** 648.4±129.7 **(84.6)** 5221.6±13.6 **(5.4)**

The results show mono-modal distribution of non-functionalized bare nZVI particles (719.7 nm) in solution with 0.5 mg L^{-1} of cadmium presence. By ten-fold higher concentration of cadmium, the bare nZVI particles show multi-modal distribution with significant proportion of particles with larger diameter (947.6 nm) and aggregates (4439.8 nm). One-pot synthetized PDCA-nZVI shows differences in hydrodynamic diameter depending of molar ratio of ligand and iron. The population of larger particles was prevailing in PDCA-nZVI material of equimolar ratio (1042.1 nm) than in PDCA-nZVI of molar ratio 1/2 (577.0 nm). Nanomaterial obtained by incubation of PDCA ligand onto nZVI in equimolar ratio showed mono-modal distribution in both case, but

the mean size of particles implies pronounced aggregation. The example of incubated PDCA-nZVI 1/2 show the significant proportion of mean sized particles (667.4 and 648.4 nm) in both of cadmium solutions.

The zeta (ζ) potential values of examined systems were determined from the measured electrophoretic mobility (Table 2). At low cadmium concentration (0.5 mg L^{-1}), the zeta-potential of functionalized nZVI particles showed higher magnitudes than bare nZVI particles. The positive values were noted at higher cadmium presence and in systems that contain bare nZVI and one-pot synthetized PDCA-nZVI material. Zeta-potential of incubated PDCA-nZVI showed negative values. By comparing the obtained results with the study on Pb removal using nZVI particles [4], where the changes in surface charge was examined, we could find some common ground. This is because of very similar chemical properties of Pb and Cd. Cadmium ions in neutral and slightly acidic medium carry double positive charge. Therefore, the higher load of cadmium led to lowering of pH value of solution and particles demonstrated a positive charge, while the opposite behaviour was visible at low concentration of cadmium added.

Table 2. Zeta (ζ) potential values of nanoparticles in water solutions containing cadmium ions; γ (Cd) = 0.5 mg L^{-1} and γ (Cd) = 5 mg L^{-1}

Particles	***Bare nZVI*** **ζ / mV**	***One-pot PDCA-nZVI 1/1*** **ζ / mV**	***One-pot PDCA-nZVI 1/2*** **ζ / mV**	***Incubated PDCA-nzVI 1/1*** **ζ / mV**	***Incubated PDCA-nZVI 1/2*** **ζ / mV**
γ(Cd) 0.5 mg L^{-1}	- 19.9 ± 0.1	-15.2 ± 0.4	-10.3 ± 0.8	-14.8 ± 0.6	-11.8 ± 0.4
γ(Cd) 5 mg L^{-1}	16.4 ± 0.3	19.5 ± 0.3	20,6 ± 0.3	-7.1 ± 0.7	-33.6 ± 0.4

Boparai et al. thoroughly studied the adsorption mechanisms of cadmium removal using nZVI particles [25]. They examined adsorption through steps of surface diffusion, intraparticle diffusion and adsorption on the interior sites of particles. Their conclusion was that the intraparticle or pore diffusion is one of the rate-limiting step in adsorption. However, the surface diffusion became more important at greater random motion when its role significantly increased. By taking in mind these facts, we can explain the discrepancies in cadmium sorption onto functionalized PDCA-nZVI materials. The intraparticle diffusion is the most probably leading step during sorption at low concentration range of cadmium, while the rise in cadmium concentration caused the prevailing surface diffusion. The size and shape of particles are the additional factors that influenced the adsorption processes [31, 33]. Bare nZVI particles consisted of longer chain-like structures and this imply the higher rate of intraparticle diffusion at low concentration of cadmium. It can be derived that the intraparticle diffusion is lower in aggregates of smaller and ellipsoidal particles we obtained from one-pot synthetized PDCA-nZVI 1/2. For this reason, they showed saturation effect at lower cadmium concentration than larger one-pot synthetized PDCA-nZVI 1/1. Moreover, the core-shell structure of functionalized PDCA-nZVI materials with magnetite and feroxyhyte layers on iron surface obviously influenced the adsorption of low cadmium content in water solution [30]. This might explain the observed discrepancies in sorption of cadmium below concentration of 5 mg L^{-1}. By rising of cadmium concentration, the surface diffusion is prevailing step in all of the examined materials and therefore, the differences in sorption were negligible.

Conclusion

The low-cost method using one-pot synthesis of functionalized zero-valent iron nanoparticles at ambient air conditions was performed in this work. The addition of dipicolinic acid as a capping reagent produced the nanoparticles of different shape and size. Such occurrence depends on molar ratio of PDCA and iron in starting solutions. Using equimolar ratio of reactants (1/1), the produced particles appeared as a spheres, which were attached mutually in short-chains. The molar ratio of PDCA to iron of 1/2 resulted with formation of aggregates of ellipsoidal particles. The fast oxidation process led to formation of magnetite and feroxyhyte oxide shell on the iron core of functionalized particles, while the bare nZVI particles demonstrated the core structure build-up of α-Fe. The synthetized materials were applied in adsorption tests of cadmium ions removal from water solution. The differences in adsorption rate of one-pot synthetized PDCA-nZVI and the PDCA-nZVI obtained by incubation were observed. Discrepancies were noted at cadmium presence below concentration of 5 mg L^{-1}. In this range, one-pot synthetized material was found to be more efficient in removal of cadmium content from water solution. The functionalization of nZVI by dipicolinic acid affected the step of intraparticle diffusion during adsorption process. Therefore, the overall adsorption of cadmium is related to different oxide layers of core-shell structure of particles along with their shape and size.

Acknowledgments

The investigation was funded by Faculty of Science, University of Zagreb and it was performed as a part of project “Analyses” (S. Rončević, principal investigator). The

authors are very grateful to our colleagues Tea Zubin Ferri and Dubravka Matković Čalogović for their generous help and assistance in SEM and XRD studies.

ORCID® iDs

Sanda Rončević – https://orcid.org/0000-0002-1899-6382

References

1. Li, S.; Wang, W.; Zhang, W. X. *J. Hazard. Mat,* **2017,** *322,* 163-171.
2. Fang, Y.; Wen, J.; Zeng, G.; Shen, M.; Cao, W.; Gong, J.; Zhang, Y. *Environ. Sci. Pollut. Res.,* **2018,** *25*, 6175-6195.
3. Wu, Y.; Pang, H.; Liu, Y.; Wang, X.; Yu, S.; Fu, D.; Chen, J.; Wang, X. Environ. Pollut. **2019,** *246*, 608-620.
4. Ahmed, M. A.; Bishay, S. T.; Ahmed, F. M.; El-Dek, S. I. *Appl. Nanosci.,* **2017,** *7*, 407-416.
5. Chekli, L.; Bayatsarmadi, B.; Sekine, R.; Sarkar, B.; Shen, A. M.; Scheckel, K. G.; Skinner, W.; Naidu, R.; Shon, H. K.; Lombi, E.; Donner, E. *Anal. Chim. Acta,* **2016**, *903*,13-35.
6. Xi, Y.; Mallavarapu, M.; Naidu, R. *Mater. Res. Bull.,* **2010**, *45*, 1361-1367.
7. Kim, C.; Ahn, J. Y.; Hwang, K. Y.; Kim, H. S.; Kwon, D. Y.; Hwang, I. *Desalin. Water Treat.,* **2015**, *54*, 1281-1289.
8. Liu, A.; Liu, J.; Han, J.; Zhang, W. X. *J. Hazard. Mat.,* **2016**, *322*, 129-135.
9. Danila, V.; Vasarevicius, S.; Valskys, V. *Energy Procedia*, **2018**, *147*, 214-219.

10. Feng, Z.; Zhu, S.; Martinis de Godoi, D. R.; Samia, A. C. S.; Scherson, D. *Anal. Chem.,* **2012**, *84*, 3764-3770.
11. Zhou, Q.; Lei, M.; Liu, Y.; Yuan, Y. *Talanta,* **2017**, *175*, 194-199.
12. Behrens, S. *Nanoscale,* **2011**, *3*, 877-892.
13. Gao, P.F.; Zhang, X. W.; Kuang, H. Z.; Li, Q. Q.; Li, Y. *IOP Conf. Series: Earth and Environmental Science 146*, **2018**, 012068 doi :10.1088/1755-1315/146/1/012068
14. McGillicuddy, N.; Nesterenko, E. P.; Nesterenko, P. N.; Jones, P., Paull, B. *J. Chromatograph. A,* **2013**,*1276*,102-111.
15. Michalski, R. *Separations,* **2018**, *5*, 16; doi:10.3390/separations5010016
16. Sarzanini, C.; Bruzzoniti, M. C. *TrAC Trends Anal. Chem.,* **2001**, *20*, 304-310.
17. Celestine, M. J.; Bullock, J. L.; Boodram, S.; Rambaran, V. H.; Holder, A. A. *Rev. Inorg. Chem.,* **2015**, *35*, 57-67.
18. Gaillard, C.; Adumeau, P.; Canet, J. L.; Gautier, A.; Boyer, D.; Beaudoin, C.; Hesling, C.; Morel, L.; Mahiou, R. *J. Mater. Chem. B,* **2013**, *1*, 4306-4312.
19. Black, C. D.; Paulenova, A.; Lapka, J. K.; Babain, V. A.; Alyapyshev, M. Y. *J. Radio. Nucl. Chem.,* **2019**, *320*, 299-307.
20. Mahmoud, M. E.; Saad, E. A.; Soliman, M. A.; Abdelwahab, M.S. *Microchem. J.*, **2019**, *145*,1102-1111.
21. Zhu, K.; Chen, C.*Interface Science and Technology*, **2019**,Vol. 29. https://doi.org/10.1016/B978-0-08-102727-1.00006-6, pp 281-330.
22. Rončević, S.; Nemet, I.; Zubin Ferri, T.; Matković-Čalogović, D. *RSC Adv*., **2019**, *9*, 31043-31051.
23. Chen, Z. X.; Jin, X. Y.; Chen, Z.; Megharaj, M.; Naidu, R. *J. Colloid Interface Sci.,* **2011**, *363*, 601-607.

24. Huang, L.; Luo, F.; Chen, Z.; Megharaj, M.; Nadu, R. *Spectrochim. Acta A*, **2015**, *137*, 154-159.

25. Boparai, H. K.; Joseph, M.; O'Caroll, D. M. *J. Hazard. Mat.,* **2011**, *186*, 458-465.

26. Jolivet, J. P.; Tronc, E.; Chaneac, C. *C. R. Geosci.,* **2006**, *338*, 488-497.

27. Gilbert, F.; Refait, P.; Leveque, F.; Remazeilles, C.; Conforto, E. *J. Phys. Chem. Solids*, **2008**, *69*, 2124-2130.

28. Rečnik, A.; Nyiro-Kosa, I.; Dodony, I.; Posfai, M. *Cryst, Eng. Comm.,* **2103**, *15*, 7539-7547.

29. Garcia-Lobato, M. A.; Martinez, A. I.; Castro-Roman, M.; Falcony, C.; Escobar-Alarcon, L . *Physica B*, **2011**, *406*, 1496-1500.

30. Nishida, N.; Amagasa, S.; Kobayashi, Y.; Yamada, Y. *Appl. Surf. Sci*., **2016**, *387*, 996-1001.

31. Saffari, M. *J. Chem. Health Risks*, **2018**, *8*, 19-37.

32. Vidmar, J.; Oprčkal, P.; Milačić, R.; Mladenović, A.; Ščančar, *J. Sci. Tot. Environ.,* **2018**, *634*, 1259-1268.

33. Awual, R.; Khraisheh, M.; Alharthi, N. H.; Luqman, M.; Islam, A.; Rezaul Karim, M.; Rahman, M. M.; Khaleque, A. *Chem. Eng. J*., **2018**, *343*, 118-127.